applied sciences

MDPI

Article

Biodeterioration Assessment of a Unique Old Pharaonic Kingdom Wooden Statue Using Advanced Diagnostic Techniques

Dina M. Atwa [1], Shimaa Ibrahim [2], Chiaramaria Stani [3], Giovanni Birarda [4], Nehal Ali [5], Emam Abdullah [6], Lisa Vaccari [4], Paola Grenni [7,*], Andrea Visca [7], Yehia Badr [8] and Wafaa Soliman [8]

1 Department of Laser Interaction with Matters, Laser Institute for Research and Applications, Beni Suef University, Beni Suef P.O. Box 62517, Egypt; dina.mohamed@lira.bsu.edu.eg
2 Department of Botany, Faculty of Science, Cairo University, Giza P.O. Box 12613, Egypt; shimaa_sa3d53@yahoo.com
3 CERIC-ERIC—Central European Research Infrastructure Consortium, S.S. 14-km 163.5, AREA Science Park, Basovizza, 34149 Trieste, Italy; chiaramaria.stani@ceric-eric.eu
4 Elettra-Sincrotrone Trieste S.C.p.A., S.S. 14-km 163.5, AREA Science Park, Basovizza, 34149 Trieste, Italy; giovanni.birarda@elettra.eu (G.B.); lisa.vaccari@elettra.eu (L.V.)
5 Department of Physics and Mathematics, Faculty of Engineering, Tanta University, Tanta P.O. Box 31527, Egypt; naboulfotoh@zewailcity.edu.eg
6 Storages Museum of Pyramids Area, Projects Sector, Ministry of Tourism and Antiquities, Giza P.O. Box 12556, Egypt; emamabdallah@gmail.com
7 National Research Council, Water Research Institute, Via Salaria km 29.300, Monterotondo, 00010 Rome, Italy; andrea.visca@irsa.cnr.it
8 Department of Laser Sciences and Interactions, National Institute of Laser Enhanced Science, Cairo University, Giza P.O. Box 12613, Egypt; ybadr@niles.edu.eg (Y.B.); wafaamas@niles.edu.eg (W.S.)
* Correspondence: paola.grenni@irsa.cnr.it

Citation: Atwa, D.M.; Ibrahim, S.; Stani, C.; Birarda, G.; Ali, N.; Abdullah, E.; Vaccari, L.; Grenni, P.; Visca, A.; Badr, Y.; et al. Biodeterioration Assessment of a Unique Old Pharaonic Kingdom Wooden Statue Using Advanced Diagnostic Techniques. *Appl. Sci.* **2022**, *12*, 7020. https://doi.org/10.3390/app12147020

Academic Editor: Antonios Papadopoulos

Received: 13 June 2022
Accepted: 9 July 2022
Published: 12 July 2022

Featured Application: The interdisciplinary study performed here using physico-chemical, microbiological, and botanical methods performed on the King Djedefre wooden statue and on some surrounding burial soil samples provided key information for conservation and consolidation measures for the Egyptian statue.

Abstract: A recently discovered Egyptian wooden statue of King Djedefre was studied together with some surrounding burial soil samples for assessing the statue biodeterioration. The wooden morphological characterisation identified the hardwood *Acacia nilotica* as the wood type. X-ray diffraction, micro-FT-IR spectroscopy, and scanning electron microscopy with an X-ray spectrometer were used to evaluate the wood deterioration degree and the soil contribution in wood biodeterioration. Microbiological analyses (fluorescent in situ hybridisation and polymerase chain reaction) were also performed to detect the microbial attack on the statue. The prolonged interaction of the statue with the burial environment caused a strong wood decay due to biotic (fungi and bacteria) and abiotic factors (e.g., humidity fluctuations of the burial environment), which caused the severe cracking and collapsing of the wood structures. The analyses of the burial soil mineral composition were relevant for obtaining an overall picture of the statue deterioration. The results are useful for planning the right conservation procedures for this very particular and important wooden statue. Furthermore, analysis of the woody cell wall will help in the selection of appropriate consolidation and recovery treatments. Because the statue is a unique single piece of wood, and the morphological observations indicated that it is a bald woman in a sitting position, this statue will provide new and interesting knowledge of Egyptian culture.

Keywords: micro-FT-IR; fluorescent in situ hybridisation; weathering effect; crystallinity of cellulose; Abu-Rawash statue; burial soil analyses

1. Introduction

Under the supervision of the Egyptian Secretary of the Supreme Council of Antiquities, Dr. Mostafa Waziry, a wooden statue was discovered in Abu-Rawash site in July 2019. It was found at a 30 m high hill distant 1.8 km to the east of the pyramid and funerary complex of Djedefre, the third ruler of ancient Egypt's 4th Dynasty. The discovery was extremely important since it provides a great deal of information on the wooden culture properties of ancient Egypt [1]. Although a large proportion of the artefacts in Egypt are made in wood, very few studies report the wood deterioration as result of interference between the biotic and abiotic processes [2–4], and in particular the soil contribution in it [3]. The studies of how the abiotic factors can induce the wooden biotic deterioration of these precious objects can improve the knowledge on the processes and the possible subsequent restoration, directing the preservation treatments [2,5,6]. Archaeological wooden objects usually undergo a transformation in their chemical composition, causing physical and mechanical property changes of the wood cells [7]. These changes are generally proportionate to the contact period with the burial soil or weathering environments [8]. These changes are attributed to the oxidation and hydrolysis processes reported in several previous studies [9,10]. Buried archaeological wood is often exposed to the microbiological processes, where different types of microorganisms (mainly bacteria and microfungi) can actively attack wood depending on the soil environment [11,12]. The most destructive white-rot and brown-rot fungi may attack partially dried woods in the presence of oxygen [13–16]. Therefore, these fungi activities are relevant only for buried archaeological wood in arid regions. On the contrary, soft-rot fungi (e.g., *Ascomycetes*) usually degrade wood with higher moisture (and also lower lignin content) [17]. The oxygen and humidity conditions are typically in temperate climates, even in soil layers above the groundwater levels [18,19]. Bacteria also may play a significant role in water-saturated wood decay [20]. Bacterial attacks (by cavitation, tunnelling, and erosion [21]) can degrade buried wood more slowly than fungi. One of the most microbial destructive forms is the lignin-degrading bacteria [22], which are abundant in most wood that was wet for a considerable period in aquatic environments or buried in saturated soils [2,5]. Bacterial deterioration acts as lignocellulose structure deterioration of wood; bacteria are also able to attack the pits membranes in tracheid and ray parenchyma, resulting in a very pronounced increase in the wood porosity [23,24]. Erosion bacteria (which create depressions in the cell wall from inside the lumen) are found to attack the water-saturated wood in low-oxygen conditions in which wood-degrading fungi and other wood-degrading bacteria cannot be active [5]; this type of bacteria (mainly *Cytophaga Flavobacterium-Bacteroides* sub-group) have the ability to degrade secondary wall layers and deplete cellulose and hemicellulose from the wood [1,25]. The nature of the wooden object deterioration is therefore extremely dependent on the surrounding environments (including the soil) and is strongly influenced by its characteristics.

The impacts of soil on the ancient buried woods could be different according to their pH value and mineralogical compositions. Burial soil ecology is extremely influenced by acidity; the fungal to bacterial ratio increases as pH decreases, while rates of wood deterioration are generally reduced by increasing soil acidity [26]. Fine-textured clay soils may protect wood more than coarse sandy soils from wood absorption and occlusion in the soil matrix [26]. An accurate evaluation of the complex environmental conditions is essential for understanding the deterioration level of buried woods and, consequently, to develop their conservation strategies.

Most evaluations of degraded wood are based on physical characterisation [27,28] or microscopic methods for observing loss in wood structure, the inorganic salt presence, and collapse of the structural integrity of cell walls [1,27]. The chemical composition, especially lignin content, is also a good indicator for the degree of deterioration [29,30]. These methods are known as destructive analyses and are very time- and material-consuming. The main changes occurring in the morphological structures of ancient wood under different deterioration conditions have to be compared to standard new wood [10,31,32]. Fourier transform infrared (FT-IR) spectroscopy and X-ray diffraction technique are very useful in

proving the advanced deterioration of ancient wood polysaccharide components (cellulose, lignin, and hemicelluloses) [31]. The crystallinity index (CrI%) measurements indicate the abiotic process, with an CrI increase in the ancient wood compared to new wood; in the case of biotic processes, the CrI of aged samples is lower than in new woods [10,31–33].

The main goal of this study was to elucidate the wood type and the deterioration displayed by an unique archaeological wooden object as a consequence of the burial soil nature and the biotic factors using a multi-analytical approach [34,35]. After the botanical species characterisation, wood and soil samples were assessed using a scanning electron microscope with an energy-dispersive X-ray spectrometer (SEM-EDX) for analysing all detectable elements simultaneously. Moreover, X-ray diffraction (XRD) and Fourier Transform Infrared microspectroscopy (μ-FT-IR) investigations were used to identify the mineral composition of soil as well as the wood deterioration degree. The fluorescence in situ hybridisation (FISH) technique and polymerase chain reaction (PCR) analyses were used to detect, enumerate, and identify the microbial community on the wooden objects by keeping the characteristics of the targeted microorganisms, i.e., their morphology and cell size. Finally, the morphology of the statue was observed to figure out what it represented.

2. Materials and Methods

2.1. The Archaeological Area

Abu-Rawash is a wide archaeological area belonging to the Memphite Necropolis northern part, at the beginning of the Nile River delta, located near the Gebel el-Ghigiga (10 km southwest of Cairo, Egypt). It is situated on a calcareous plateau and occupies an area of 90 km^2, 8 km northwest of the Giza Pyramids. The area consists in sedimentary rocks, basalt flows, and loose sediments (multiple kinds of limestone, sandstone, basalt, and clay) [36,37]. Abu-Rawash is a famous site due to the presence of the pyramid of King Djedefre, the third king of the 4th Dynasty during the Old Kingdom (2566–2558 BC), which is the son and successor of the Pharaoh Cheops (Khufu) [38,39]. The area is rich in funerary and worship sites dating from the Early Dynastic to the Coptic-Christian periods (2925 BC–500 AD), which has not been deeply studied and barely excavated [40]. Several cemeteries of commoners were dug in simple oval pits or small mud-brick mastabas (flat-roofed tomb, rectangular structure with inward sloping sides, constructed out of mud bricks) dating to the Naqada III period (3200 to 3000 BC, the final and most important period of the Predynastic age) [41–43].

2.2. Statue Description

The statue is a special and unique item since it belongs to the 4th dynasty of the Old Egyptian Kingdom. It was sculptured from a single piece of wood without any connectors, indicating the primary manufacturing style, unlike the style of that era.

The statue (Figure 1) was found in the elites' cemetery of the 4th dynasty next to another stone statue that was decorated with the King Djedefre name; this suggested that the wood statue was likely owned by this 4th Dynasty king [43,44]. It was discovered in a shallow burial pit (3.5 m length × 1.7 m width × 1.5 m height). The burial pit was in bad conditions at the time of excavation, being internally collapsed and extremely water-saturated, as reported by the archaeologists.

Although it is known that the knowledge of wood moisture could be useful to determine the biodeterioration type [1,44], it was not measured at the time of the statue discovery to avoid damaging the statue (this measure in fact requires wood samples to be weighed and to be put in an oven). From the discovery up to now, the statue has been kept in the best air humidity conditions for its conservation and analyses [30] at the Grand Egyptian Museum (GEM) Conservation Lab (Cairo, Egypt).

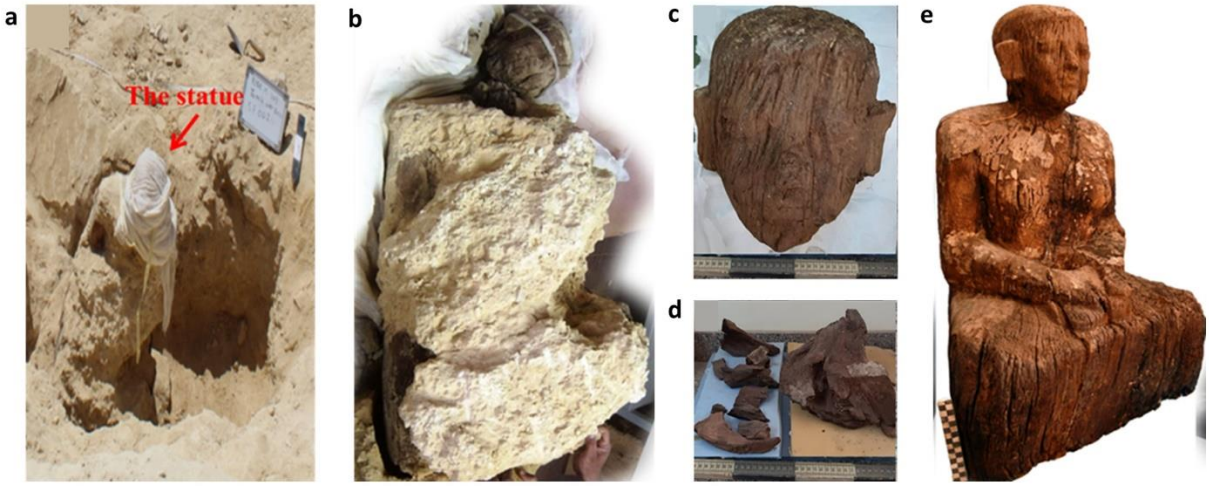

Figure 1. (**a**) The statue at the excavation site at the time of discovery. (**b**) The statue was mostly covered by a thick soil layer. (**c**) The detached head before the restoration. The facial features were not clearly recognisable. (**d**) Fallen wood fragments after soil layer removal. (**e**) The statue after a partial restoration at the Grand Egyptian Museum (GEM) Conservation Lab (Cairo, Egypt).

The statue was in extremely poor state of conservation (Figure 1a), with the head totally detached from the body. For this reason, during the dig, it was wrapped in a white fabric (Figure 1a) for keeping the fragments together. After it was completely excavated, the statue was enveloped by a tenacious and thick layer of soil (Figure 1b). The wood appeared to be heavily cracked and fragmented (Figure 1c,d). Even after an accurate reconstruction, any decoration or inscription was not visible due to wood deterioration. However, observations of the stature features were performed to comprehend what it represents and its meaning inside the Egyptian culture. The features of the face and the dress were not clearly recognisable (Figure 1c), while it was possible to reveal its shape (Figure 1e).

2.3. Sample Description and Wood Classification

Two wooden samples (#1 and #2) were collected from the fragmented inner part of the statue (Figure 2a,b).

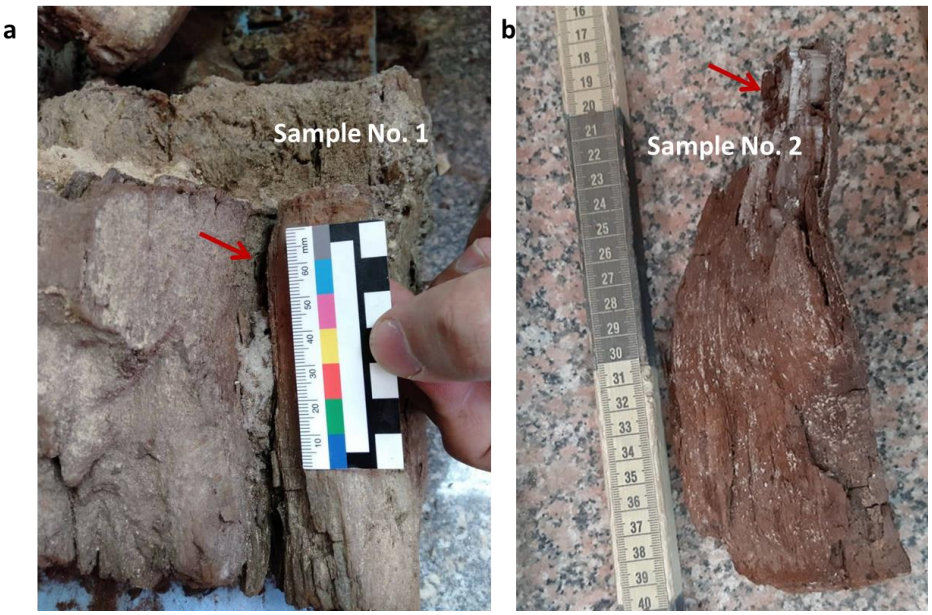

Figure 2. Sampling points (red arrows) of the archaeological wood samples #1 (**a**) and #2 (**b**).

The botanical species of the ancient wood samples was identified by the Biology Laboratory in the Institute of Conservation and Restoration (ISCR), Rome, Italy. Due to the fragility of the wood, the samples were treated with an acrylic-based thermoplastic resin in order to cut them safely into the three dimensions (transversal, tangential, and radial sections) [45,46]. The identification was carried out using a stereomicroscope (M205C, Leica) at different magnifications, referring to a wood library [47].

A fresh *Acacia nilotica* wood sample (#3) was purchased from El-Orman Botanical Garden (Giza, Egypt) for the assessment of the archaeological wood biodeterioration. Finally, three soil samples (#4, #5, and #6) were collected from different points of the thick layer removed from the statue (Figure 1b). Sample description is reported in Table 1.

Table 1. Sample numbers and description.

Samples	Description	Sampling Position	Colour
#1	Pure core wooden sample	Inner the statue	Dark brown
#2	Wood interfered with soil	Inner the statue	Light brown
#3	Standard sample (*Acacia nilotica*)	-	Fresh wood colour
#4	Soil sample	Inner the statue	Red
#5	Soil sample	Petrified outer layer	White
#6	Soil sample	Inner the statue	Dark grey

The #1 and #2 wood samples were analysed by SEM, XRD, FT-IR, and FISH tools, and in some cases compared to the standard wood sample (#3). Soil samples were characterised by XRD and FT-IR spectroscopy.

2.4. Microscopic and SEM-EDX Observations

Microscopic studies on wooden samples were performed at the Biology Laboratory in the Institute of Conservation and Restoration (ISCR), (Rome, Italy), using a stereomicroscope (M205C, Leica). At the National Research Centre (NRC, Giza, Egypt), an environmental scanning electron microscope coupled with an energy-dispersive X-ray unit (SEM-EDX) (SEM-Quanta FEG-250, ESEM, FEI, Eindhoven, The Netherlands) was used to measure the samples without any further preparation under high vacuum conditions. The images were collected using a back-scattered electron detector (BSED) with a 1.4 nm resolution at an accelerated voltage of 20 KV. SEM-EDX analyses were performed on sample #1.

2.5. X-ray Diffraction (XDR)

XRD measurements were performed at the Egyptian National Institute of Standards in Giza (Egypt). The soil and ancient wood samples were grinded using an agate mortar for obtaining 5–10-micron grain size, while the sample of standard wood was analysed without any sample preparation due to grinding difficulty. The X-ray diffractometer system (PANalytical, X'Pert Pro, PW 3040/60 model) was used, with a Cu anode, working at 30 mA/40 kV at a 25 °C with a step size (2Θ) of 0.033. An X-ray tube produced a monochromatic Cu Kα radiation of wavelength 0.154 nm, recorded from (2Θ) 5° to 70° in the case of samples #1, #2, #4, #5, and #6 and from 5° to 30° in the case of wooden sample #1 and sample #3 for measuring the crystallinity index of cellulose (CrI%). For this purpose, the Segal formula (Equation (1)) was used [48–51]:

$$\mathrm{CrI\%} = 100\frac{I\,(200) - I\,(am)}{I\,(200)} \quad (1)$$

where $I\,(am)$ is the minimum intensity between (101) and (200) diffraction peaks at (2Θ) value 18.04° and it is attributed to the amorphous cellulosic fibres. (I_{101}) and (I_{200}) are the

diffraction peak intensities regarding the crystalline cellulose where (I_{200}) is the highest peak at (2Θ) 22.2°.

X'Pert high score data acquisition and an interpretation software (Malvern PANalytical, Malvern, UK) were used for interpreting the results.

CrI% of the #1 and #3 wood samples was calculated by subtracting the minimum intensity of peak 101 (*I am*), characteristic of the amorphous wood components, from the maximum intensity of peak 200 (*I c*) representing the crystalline portions and then taking the ratio between the difference to the total intensity at 200 peak.

2.6. Micro-FT-IR Spectroscopy

The microspectroscopy FT-IR measurements (μ-FT-IR) were performed at the Chemical and Life Sciences branch of the SISSI beamline at Elettra Sincrotrone, (Trieste, Italy), using published methods [52].

Two small flakes of wood were collected from both the ancient wooden samples (#1 and #2). The flakes were pressed using a diamond compression cell (Diamond EX press by S.T. Japan, clear aperture 1.6 mm) to flatten them to a thickness suitable for FT-IR measurements in transmission mode. After this procedure, the diamond compression cell was opened, and the infrared images were collected on the exposed face of the compression cell by a Vis-IR Bruker Hyperion 3000 microscope coupled with the Vertex 70v interferometer in the mid-infrared range (Mid-IR) with a focal plane array (FPA) detector. The spectral range was between 3950 and 900 cm^{-1}, collecting 256 scans at 4 cm^{-1}. The same procedures were also applied for the *Acacia* standard wood sample (#3). An FPA mosaic of 6 tiles (2 × 3) was acquired on sample #1, while 9 tiles (3 × 3) were collected for sample #2. Considering 4096 spectra for each tile, a total amount of 61,440 spectra were acquired on the two samples. A single FPA image was collected for the standard wood sample.

Soil samples (#4, #5, and #6) were also analysed to evaluate their mineral composition, with the same condition described above.

The μ-FT-IR data set was analysed by OPUS 7.5 software. FPA maps were firstly compensated for atmospheric contribution (water vapour and CO_2) and baselined. The spectra were also pre-processed by the Quasar open-source software (https://quasar.codes, accessed on 10 January 2020). All the empty pixels (absorbance < 0.01) were removed. Averaged spectra were extracted from the mosaic of each wood sample and compared with the wood standard. Then, the integral areas of the bands in the 1180–930 cm^{-1}, 1530–1480 cm^{-1}, and 1800–1530 cm^{-1} ranges were calculated for both ancient wood samples (#1 and #2) and the standard one (#3) in order to visualise the distribution of cellulose, lignin, and deterioration products, respectively. Statistical calculations were performed on the processed data (by Origin Pro 2020 9.7 software, Origin Lab, Ltd., Northampton, MA, USA). The obtained values were normalised against the wood standard sample. To compare the ancient wood samples with the standard one, the scales of the FPA false colour maps were calibrated from blue (low intensity) to red (high intensity) to the highest mean value of integration recorded (usually from the standard sample, with the exception of the band due to the deterioration products where the highest value was reached by the sample #1).

2.7. Microbial Analyses by Fluorescent In Situ Hybridisation (FISH)

FISH was performed directly on microbiological samples taken from the archaeological wooden samples #1 using a piece of an adhesive tape (Fungi-tape; Cat. number: SDL745; KEY SCIENTIFIC, Stamford, TX, USA), applying little pieces of them on the wooden surface [53]. Because the number of microbial cells on the tape were very low for observing them under the epifluorescence microscope, tape piece was immediately placed in the 1× YT broth (BP2467-500; Fisher Scientific, Vantaa, Finland) liquid media (containing per litre 10 g of tryptone, 5 g of yeast extract, 5 g of glucose, and 5 g of sodium chloride; pH 7.0 and previously sterilised) for bacterial cultivation (overnight at 37 °C) in a shaking incubator. After one night, some filters (Millipore polycarbonate filters; pore size 0.2 μm; Ø 25 mm) were prepared for FISH analysis. Before FISH, cell fixation was carried out in a buffer (4%

paraformaldehyde in PBS, pH 7.2) and incubated for 3 h at 4 °C. After the fixation, filters were washed in PBS and stored in 1:1 (*v*/*v*) PBS/ethanol at −20 °C. FISH was performed following published procedures [54,55]. Briefly, filters were dehydrated by successive passages in 50%, 80%, and 95% ethanol series (3 min each). For hybridisation, 150 µL of hybridisation solution (0.9 M NaCl, 20 mM Tris HCl, 0.1% SDS, formamide) was mixed with 15 µL (50 ng) of each oligonucleotide FISH probe. After hybridisation, samples were placed in a washing solution (180 mM NaCl, 20 mM Tris–HCl (pH 7.2), 0.1% SDS, 5 mM EDTA) for 30 min at 48 °C and then rinsed with distilled water. Two oligonucleotide probes (EUB: 5′-GCTGCCTCCCGTAGGAGT-3′; *Archaea*: 5′-GTGCTCCCCCGCCAATTCCT-3′) labelled with different fluorochromes (CY3 or FLU) were used (MWG AG Biotech, Germany). Other information is available at https://probebase.csb.univie.ac.at (accessed 10 October 2021) [56]. Fluorescent staining was also performed with 4′,6-diamidino-2-phenylindole (DAPI) for 10 min, rinsed with distilled water, and air-dried. Slides were observed with an epifluorescence microscope (Leica DM 4000B, Leica Microsystems GmbH, Wetzlar, Germany) equipped with a 50 W mercury lamp HBO and a different combination of filters at 1000× magnification. Image caption was carried out with a CCD camera.

2.8. DNA Extraction and qPCR Analysis

DNA was extracted from bacterial cultivations (see the previous paragraph) using the DNeasy PowerSoil Kit and DNeasy Plant Mini Kit (QIAGEN GmbH, Hilden, Germany) according to the manufacturer's protocol. The extraction yield and quality of the DNA were spectrophotometrically assessed (MultiSkan Sky Microplate Spectrophotometer, Thermo Fisher Scientific, Waltham, MA, USA).

The extracted DNA was amplified by PCR by CFX96 real-time PCR detection system (Bio-Rad, Hercules, CA, USA) using the SYBR Green detection and targeting 16S rRNA gene of Prokaryote (Fw: 5′-CGGTGAATACGTTCYCGG-3′; Rv: 5′-TACCTTGTTACGACTT-3′) [57] and *Bacteria* (Fw: 5′-ACTCCTACGGGAGGCAGCAG-3′; Rv: 5′-ATTACCGC GGCTGCTGG-3′) [58]. Each reaction was carried out in a total volume of 20 µL containing 10 µL SsoAdvanced Universal SYBR Green Supermix (Bio-Rad, Hercules, CA, USA), 0.5 µL of each primer (10 µM), and 15 ng of DNA template. The thermal cycling conditions were as follows: 95 °C for 3 min, 45 cycles at 95 °C for 15 s, annealing temperature (Tm) specific for each primer pair for 30 s, and 72 °C for 30 s. The fluorescence signal was read after each elongation step. All reactions were terminated with a melting curve starting at 55 °C and increasing by 0.5 °C until 95 °C to verify amplicon specificity. Each assay was run in triplicate including the no template controls (NTC).

3. Results

3.1. Wood Classification and Statue Features

The botanical species of the ancient wood samples was identified as *Acacia nilotica*, a national wood species [59]. This type of wood was commonly used for wooden objects of ancient Egypt [60]. The observations of the statue let us know that the statue represents a commoner bald woman with crossed hands, overlapping, in a sitting position. It measured 94 cm height × 47 cm (shoulder width). It was similar to a typical ancient Egyptian seated scribe [61].

3.2. Soil Characterisation and Its Interaction with Ancient Wood

Data on µ-FT-IR spectroscopy analyses for soil samples (#4, #5, and #6) are reported in Figure S1. The coloured selections highlight the characteristic infrared features of carbonates, sulphates, and silicate. Among silicates, the presence of kaolinite can be distinguished by the sharp absorptions in the 3750–3500 cm^{-1} range.

Optical images collected by the stereomicroscope (Figure 3) showed soil particulates deeply penetrate the wood fragments (Figure 3a,b).

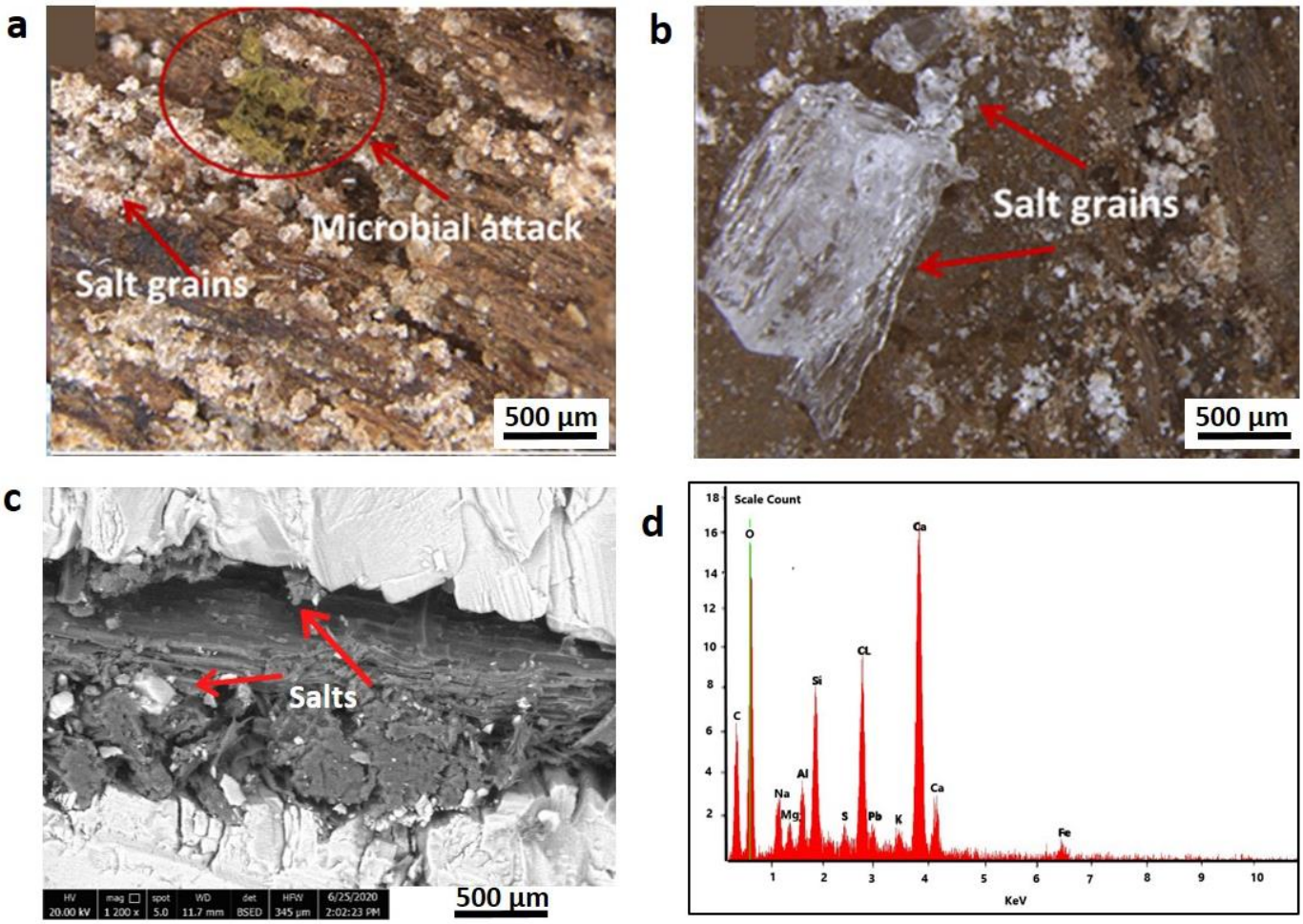

Figure 3. (**a**,**b**) Stereomicroscopic images (40× magnification) of wood samples #1 (pure core wooden sample) and #2 (wood interfered with soil), of the ancient statue, respectively. Salt grains and a microbial attack are visible. (**c**) SEM image (magnification 1200×) of sample #2 shows the crystalised salt dispersed on the wood sample. (**d**) EDX average spectrum of sample #1.

The presence of thick layers of soil enveloping the wood of sample #2 together with diffuse mineral grains were clearly observed in the SEM images (Figure 3c). SEM-EDX spectrum (Figure 3d, wood sample #1) shows the presence of very high amount of Ca, Cl, and Si and lower amounts of Na, Mg, Al, S, K, Pb, and Fe; this might be attributed to the penetration of soil components inside the wood, as these elements are the main soil constituents [62].

The XRD patterns of archaeological wood samples #1 and #2 (Figure 4a,b with 2Θ values at 31.72°, 45.46°, and 56.48°) showed a great amount of halite, a sodium chloride salt, commonly known as the "rock salt".

Moreover, both XRD and FT-IR analyses revealed the presence of weddellite ($CaC_2O_4 \cdot 2H_2O$), a calcium oxalate compound, especially in wood sample #1 (Figure 4a with 2oth XRD and FT-IR analyses revealed the presence of weddellitevalues at 14.33°, 32.22°, and 20.09°). As shown in Figure 4d, false-colour FPA mosaic showed some hot spots obtained by integrating the sharp absorption peak at 1320 cm^{-1} (Figure 4e). An average spectrum was extracted from one of the points and compared to a reference value (Figure 4e). No weddellite crystals were observed in sample #2. XRD measurements on the soil samples #4, #5, and #6 confirmed they are mainly composed by halite (NaCl), quartz (SiO_2), and kaolinite (($Al_2Si_2O_5$ $(OH)_4$) almost in the same proportions.

In addition, sample #5 (the soil sample of the petrified outer soil layer) revealed a certain amount of calcite ($CaCO_3$) and gypsum ($CaSO_4 \cdot 2H_2O$), while sample #6 (soil sample

from the inner part of the statue) also contained periclase (MgO), a mineral occurring in limestone and marble (Figure S2). Detailed XRD results on wood and soil samples are reported in Table S1.

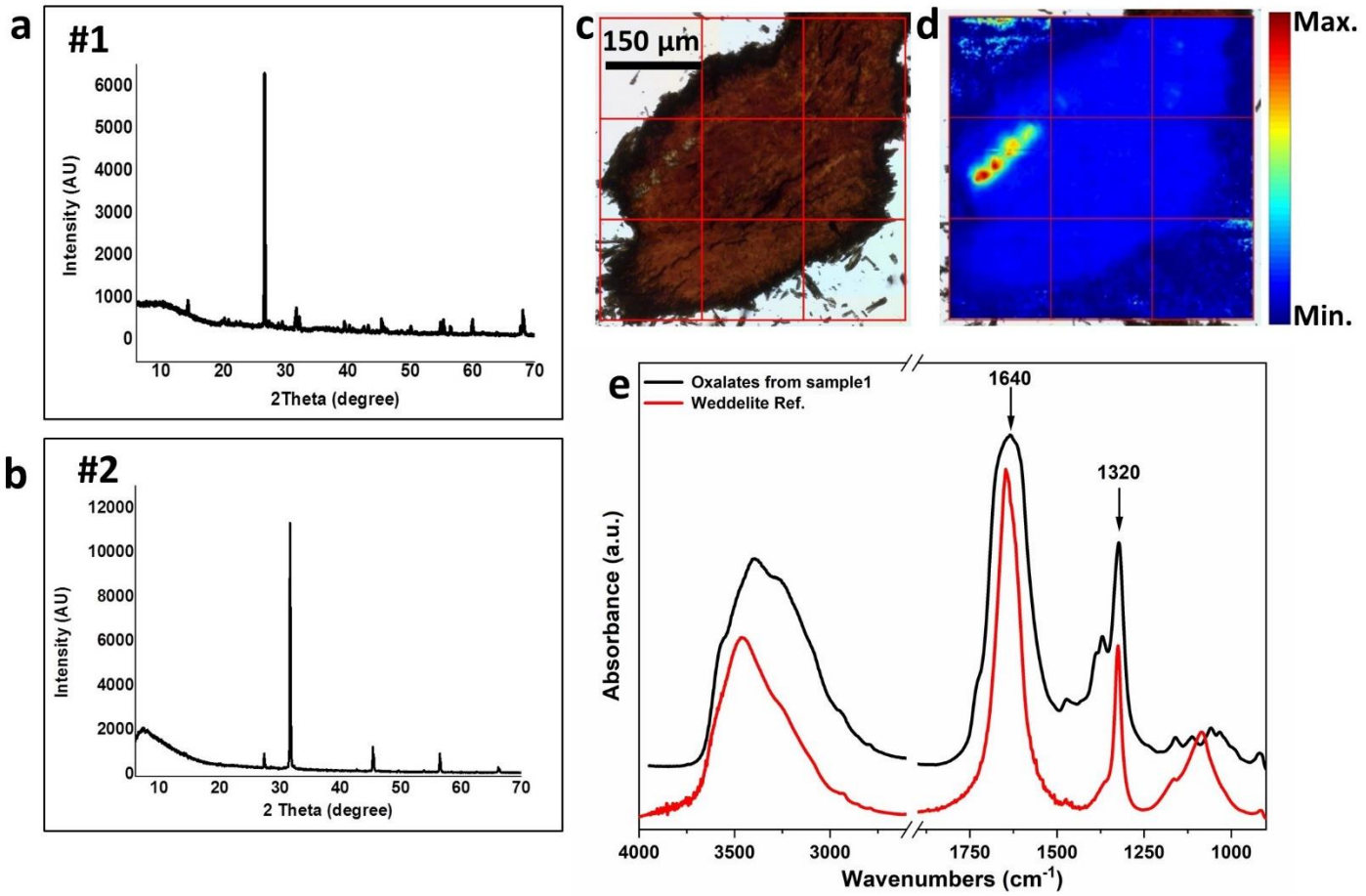

Figure 4. (**a**,**b**) XRD patterns of wood samples #1 and #2 of the archaeological statue, respectively, with a 2Θ value (2 Theta) from 5° to 70°. (**c**) Optical image of the sample #1. The red grid represents the area measured by Infrared focal plane array (FPA) detector shown then in panel d. (**d**) False-colour map of the sample #1 obtained by integrating the oxalate band in the 1350–1300 cm^{-1} range (see panel e). This map highlights the distribution of oxalates within the sample #1 (blue corresponds to lowest amount, red to the highest one, see the colour bar aside for reference). (**e**) Average spectrum of oxalates (black line) extracted from the hot spots (bright red) highlighted in the false-colour FPA map in panel d. It is compared with a weddellite reference spectrum (Weddelite ref., red line) obtained from the Kimmel Center for Archaeological Science Infrared Standards Library, Weizmann Institute of Science (Rehovot, Israel).

3.3. Bacterial and Fungi Presence

As highlighted by the red circle in Figure 3a, a possible biological attack was observed on the wood fragment where sample #1 was collected.

SEM images of wood samples #1 showed a microbial (fungal) attack (Figure 5a,b). In particular, long hyphae were observed in panel (a), while several fungal spores are visible in Figure 5b.

On the other hand, FISH analysis revealed an overall presence of *Bacteria* in the analysed sample #1. The Archaea probe did not provide positive signals under the epifluorescence microscope. The microbiological samples were composed mainly of cells with bacilli in shape, with four bacterial cells (or their multiples) in each chain. PCR analysis confirmed the presence of *Bacteria* ($1.65 \times 10^{11} \pm 2.3 \times 10^{10}$ copies of 16S *rRNA* gene) and *Prokaryota* ($2.52 \times 10^{11} \pm 1.2 \times 10^{10}$ copies of 16S *rRNA* gene). Figure 5c,d shows

images of FISH assays under the epifluorescence microscope using the DAPI-stain (blue) and Cy3-labelled EUB probe (in red) for *Bacteria*.

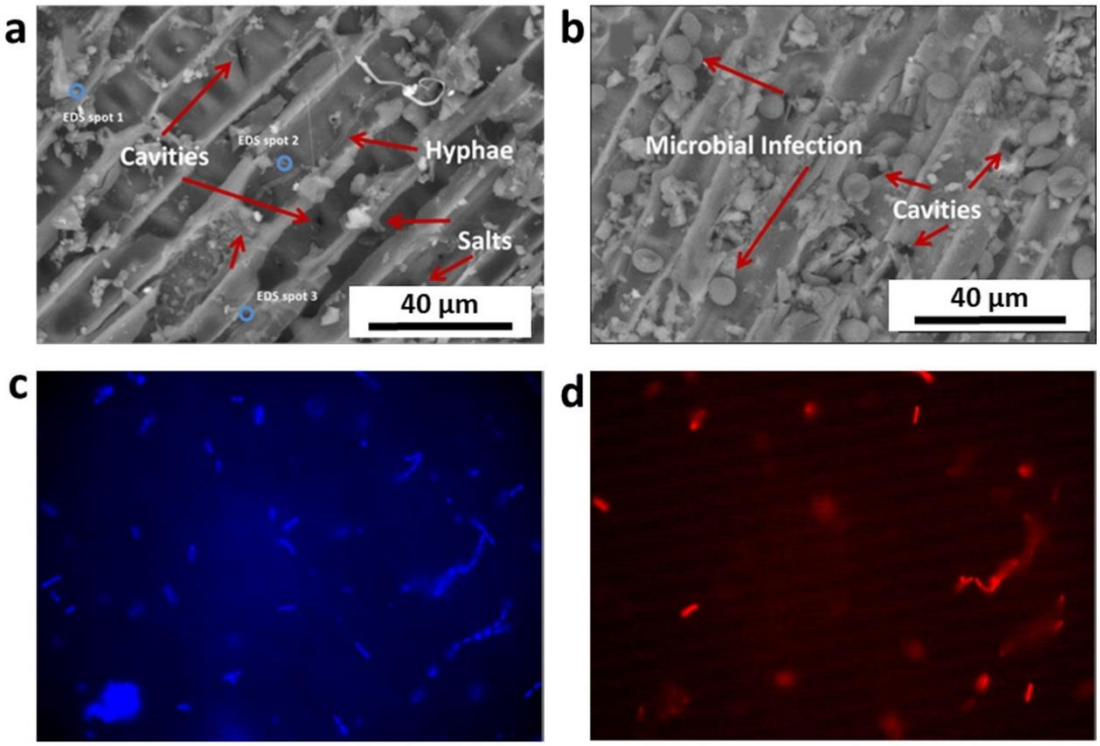

Figure 5. (**a**,**b**) SEM images (magnification 3000×) of sample #1 (pure core wooden sample, inner the statue). Fungal hyphae (panel (**a**)) and spores (panel (**b**)) are visible. (**c**,**d**) Images of FISH assays under the epifluorescence microscope using the DAPI-stain for all microbial cells (blue, panel (**c**)) and the Cy3-labelled EUB probe for *Bacteria* (red, panel (**d**)) (magnification 1000×).

3.4. Wood Deterioration

SEM image in Figure 6a is a transverse section of *Acacia nilotica* standard sample. This diffuse-porous wood is characterised by solitary or multiples vessels. Axial parenchyma was vasicentric, aliform lozenge-aliform, and confluent where the homogeneous structure of wood cell walls clearly appeared. On the contrary, the ancient wood sample #1 (Figure 6b) showed an advanced decay in which a wide wood fragmentation was visible. Cell walls look collapsed, and cracked vessels and voids were clearly observable. This led to a porosity and fragility of the wood structure. Such wood cells separations might be attributed to the collapse of middle lamella region that leads to reduction in the homogeneity of the wood structure, causing either fracture or evacuation and cell wall erosion [63].

XRD patterns of the standard sample compared with sample #1 from (2Θ) 5° to 30° are displayed in Figure 7a. The standard sample shows two diffraction peaks at (2Θ) 15.5° (101) and 22.2° (200), characteristic of the *Acacia nilotica* natural fibres [64]. The aforementioned two peaks are attributed to the cellulose I typical crystallographic plane. In sample #1, the intensity of the two above-mentioned main peaks strongly decreased, while a further weak peak appeared at (2Θ) 18.04°, that is, the minimum intensity between the above-mentioned peaks; it is usually attributed to the amorphous fractions of lignin, pectins, hemicellulose, and amorphous cellulose.

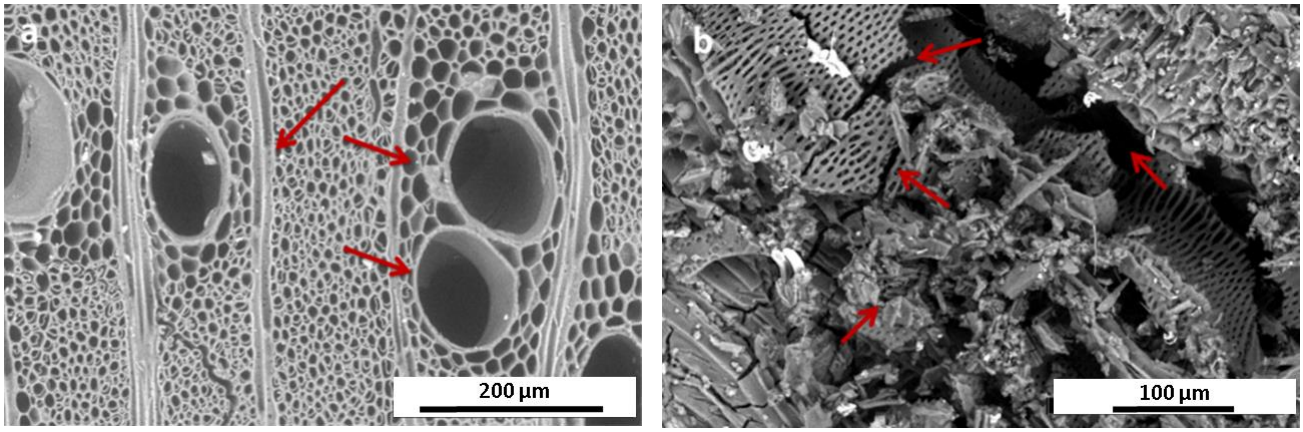

Figure 6. (**a**) SEM image of the *Acacia* standard wood sample (magnification 600×); red arrows indicate the homogeneous structure of wood cell walls. (**b**) SEM image of the sample #1 (Pure core wooden sample; magnification 800×). The red arrows indicate the strongly fragmented wood structure.

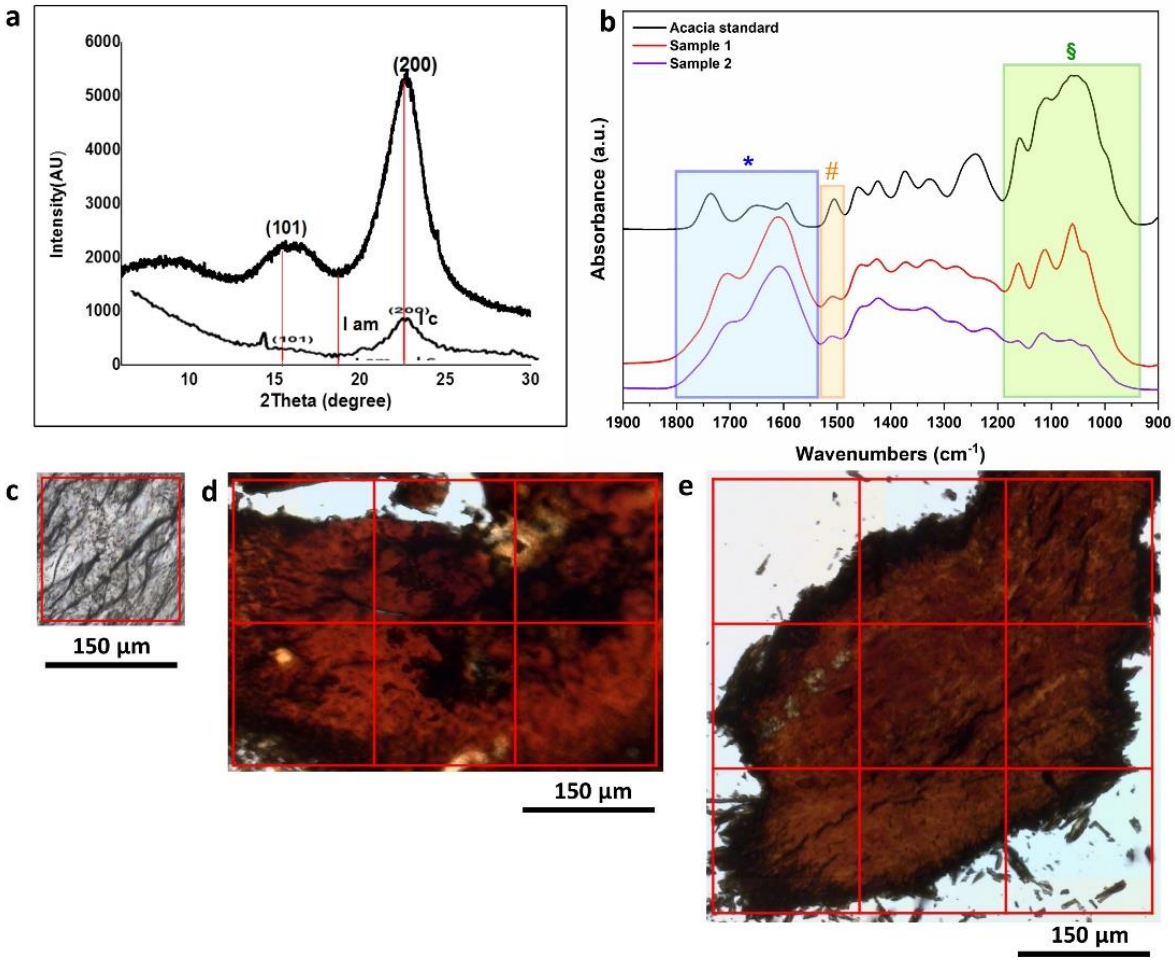

Figure 7. (**a**) XRD patterns of the standard wood sample (thicker upper line) and of the archaeological wood sample #1. (**b**) Average spectra extracted from the FPA images of *Acacia* standard sample (black line), sample #1, and sample #2 (red and violet lines, respectively). The coloured rectangles highlight the infrared features of interest for cellulose (§), lignin (#), and deterioration products (*) (green, orange, and blue, respectively). (**c**–**e**) Optical images (15×) of the *Acacia* standard sample (**c**), sample #1 (**d**), and sample #2 (**e**), obtained with the VIS-IR microscope.

The crystallinity index (CrI %), calculated by means of the Segal empirical method, was found to be 67.2% for the *Acacia* standard sample and 37.7% for the sample #1. The crystallinity index in sample #2 was not measured because the very high amount of inorganic material did not allow to obtain a significant result.

The optical images of the *Acacia* standard sample and the ancient wood samples #1 and #2 collected by the infrared microscope are shown in Figure 7c–e. The *Acacia* standard sample showed a clear colour and a homogeneous appearance. Well-preserved parallel wood fibres were observed, even after the compression of the sample in the diamond cell. The ancient samples, on the contrary, showed a deep brown/reddish colour and an amorphous appearance, and wood structures were not distinguished, also due to the preparation of the sample (its compression in the diamond cell).

Figure 7b shows the average spectra of the *Acacia* standard (pink line) and the two fragments of ancient wood samples #1 and #2 (green and red lines, respectively) in the fingerprint region (1900–900 cm^{-1}). The latter shows the characteristic infrared features of woods, but with some significant differences if compared with the standard one.

The broad band in the 1180–930 cm^{-1} range (Figure 7b, green rectangular selection labelled with §) is attributed to C-O, C-O-C, and C-C stretching vibrations of carbohydrates and can be assigned to the presence of cellulose and hemicellulose [63]. This band shows a very intense signal with a broad shape in the standard wood. In sample #1, a slight decrease in the absorption signal was accompanied by a sharpening of the infrared features, while sample #2 showed a further decrease in the intensity with a strong loss of the characteristic band shape.

The bands at 1509 cm^{-1} (Figure 7b, orange rectangular selection labelled with #) can be attributed to C=C stretching in guaiacyl rings, one of the main moieties of lignin, and were used for mapping the distribution of this wood component [65].

A decrease in the signal of this band was observed for both samples #1 and #2. In the spectral range of 1480–1180 cm^{-1}, several infrared features were present. They can be assigned to both cellulose/hemicellulose (i.e., the band at around 1320 cm^{-1} was due to the C-H bending of this molecule) and lignin (i.e., the band at around 1270 cm^{-1} was attributed to C–O stretching) [30]. This spectral range showed a broadening and a decrease in the infrared feature definition that can be linked to a decrease in the structural order of the wooden tissues in the archaeological woods when compared to the standard one. This had already been observed by several authors [30,66].

Finally, a strong increase in the infrared signal in the 1800–1530 cm^{-1} range was detected in the archaeological wood fragments when compared to the *Acacia* one (Figure 7b, blue rectangular selection labelled with ✻). Infrared features in this range are usually attributed to C=O stretching vibrations of esters, ketones, and aldehydes (in particular at higher frequencies). Moreover, the bending vibrations of -OH and the COO^{-} stretching vibrations can fall at around 1640 and 1600 cm^{-1}, respectively.

The spectrum of the standard wood (Figure 7b, black line) showed a peak at around 1730 cm^{-1}. It shifted at around 1711 cm^{-1} in the #1 and #2 samples, while the broad peak at about 1610 cm^{-1} strongly increased in intensity in the ancient samples. These bands could have been due to carbonyl stretching vibrations in carboxylic acids and carboxylic acid salts and can be attributed to a wood deterioration product increase originating from both hydrolysis and oxidative processes of cellulose [63,67]. The above-mentioned bands are fundamental for observing the distribution and to quantify the relative percentages of cellulose, lignin, and their deterioration products in the archaeological woods.

Unfortunately, the intense peak of weddellite at 1640 cm^{-1} (Figure 4e) perfectly matched in the 1800–1530 cm^{-1} range, with the band identified to be diagnostic of the formation of wood deterioration products.

To avoid an overestimation of the deterioration product presence, the pixels corresponding to the oxalate crystals in sample #1 were cut out by the Quasar software [52]. Then, the FPA false colour maps (Figure 8a) were obtained by integrating the areas of the

bands attributed to cellulose, lignin, and the deterioration products as described above and highlighted by the rectangular selections in Figure 7b.

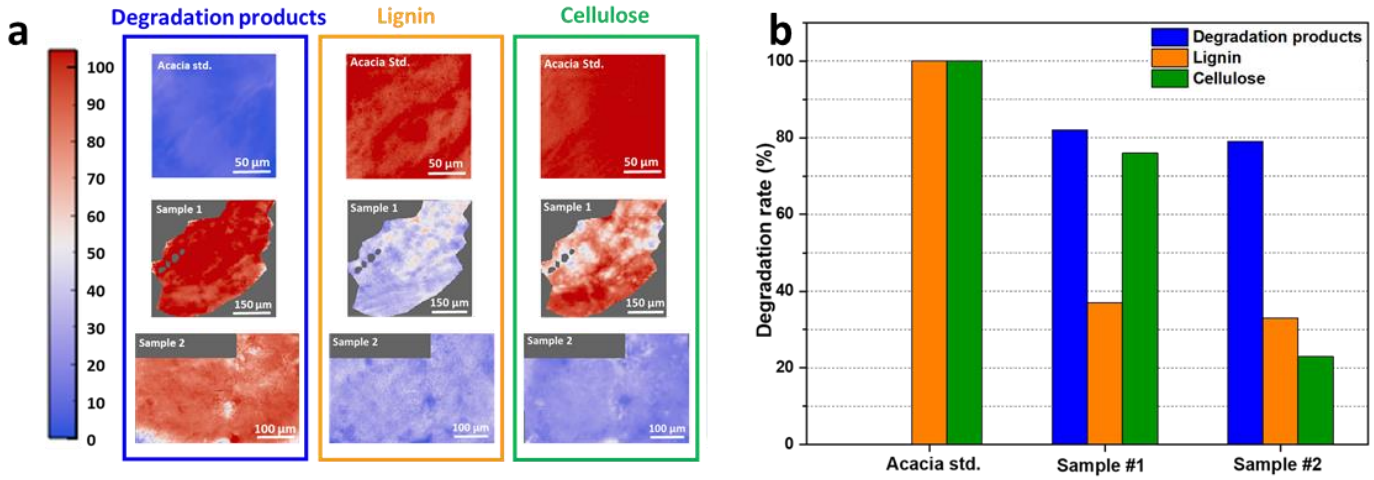

Figure 8. (**a**) FPA mosaic of samples # 1 and #2 (archaeological wooden samples) and *Acacia* standard (#3). The FPA map scale (blue: low intensity; red: high intensity) was calibrated to the highest mean values of integration recorded. The false-colour map was obtained by integrating the oxalate band in the range 1350–1300 cm^{-1}. (**b**) Average spectrum of oxalates extracted from the hot spots highlighted in the false-colour FPA map (panel (**a**)). It was compared with a Weddellite reference spectrum from the Kimmel Center for Archaeological Science Infrared Standards Library, Weizmann Institute of Science (Rehovot, Israel).

As expected, as shown in Figure 8a, the false-colour FPA images of the *Acacia* standard sample showed the highest amounts (corresponding to the red colour in the maps and the scale bar) of cellulose and lignin (Figure 8b, orange and green rectangles, respectively) and the lower amount of deterioration products (Figure 8a, blue rectangle). The FPA map of sample #1 for cellulose still showed a good preservation and a wide distribution with only some degraded regions (blue spots), while the lignin content was quite low with only some preserved pale red spots [13].

Interestingly, lignin red spots almost co-localised with some intense cellulose ones, while the pale red regions in the deterioration products map corresponded with the most intense red spots in the cellulose one. This let us postulate that the formation of the deterioration products could be mainly linked to the lignin content decrease. In sample #2, on the other hand, a very strong decrease in cellulose and lignin contents was observed, followed by a homogeneous deterioration product increase. An estimation of the percentage decrease in cellulose and lignin in samples #1 and #2 in comparison to the *Acacia* standard sample was performed (Figure 8b). The deterioration levels were defined as weak (from 0 to 33 % of decrease), moderate (from 34 to 66% of decrease), and severe (from 67 to 100% of decrease) [29,68]. Sample #1 showed a weak (−24%) cellulose deterioration and a moderate/severe (−63%) lignin degradation, while sample #2 showed a severe degradation for both cellulose (−77%) and lignin (−67%) (Figure 8b, green and orange columns for cellulose and lignin, respectively). On the contrary, the amount of deterioration products was attested around the 80% for both samples #1 and #2 (Figure 8b, blue column).

4. Discussion

Unlike the knowledge on the 4th dynasty manufacturing styles, where imported wood species were used for elites' properties and the manufacturing techniques were also developed [69], the statue was a royal property made of a single piece of a national wood (*Acacia nilotica*) with a poor manufacturing style. This may indicate the limited trade routes between ancient Egypt and neighbouring countries, particularly for that era, probably due to a political reason [70].

The observations of the statue and its comparison with the artistic feature descriptions of Egyptian sculpture art in the Old Kingdom let us know that the statue embodied a commoner bald woman [71,72]. This fact was unexpected because the sculptors in ancient Egypt did not depict bald statues, except for male priests, as reported by several authors [73,74]. In ancient Egypt, priesthoods (which had a variety of different functionaries) were usually represented without hair [75]. Women were sometimes included at the head of groups making daily offerings to the gods in their role as musician priestesses [76]. This discovered statute could change the knowledge about priesthood of that era, suggesting that also commoner women may perhaps have belonged to the caste of priests and performed the same efforts of men. Therefore, the discovery of this statue may change the prevailing thought about religious life in ancient Egypt [77]. The sitting position of the statue is also very interesting—it is similar to an ancient Egyptian seated scribe. The scribe had a great value in ancient Egypt due to his great role in codifying the various sciences as well as other documents concerning the affairs of government and all walks of life [78]. This gives us the indication that this statue belongs to a common woman who worked as a priestly writer, and the sculptor deliberately carved it in the form of a priest sitting and writing. These findings have to be, in any case, confirmed with more in-depth studies.

The nature of the pit where the statue was discovered made it an interesting case of study. In fact, it was found at a shallow level of a collapsed and damp pit, not in a burial chamber (as usually found for other items [79]), which made it vulnerable to many factors of biotic and abiotic damage.

The prolonged interaction of the statue with the burial environment caused strong wood deterioration as a consequence of a complex combination of biotic and abiotic factors [80]. Among the biotic factors, fungi and bacteria clearly detected by both SEM and FISH analyses caused a deterioration of the main wood components. XRD measurements revealed a strong decrease in cellulose crystallinity (less than about 43.9%) complemented by an increase in the amorphous components. A strong decrease in lignin and cellulose were detected for both the analysed ancient wooden samples collected from the statue (#1: pure core wooden sample; #2: wood sample interfered with soil), as shown by μ-FT-IR measurements. The lignin showed the highest rate of deterioration in both samples, while cellulose was partially better preserved in sample #1. Moreover, the advanced decay of the wood composing the statue was also revealed by the detection of an intense increase in the infrared absorption band at 1610 cm^{-1} [81]. This band is normally due to organic acid presence derived from the main wood component deterioration as a consequence of a biological attack. For example, fungi can play an important role in deterioration, especially producing oxalic acid as a secondary product of their metabolism [82].

Both XRD and FT-IR measurements revealed the presence of weddellite, a calcium oxalate mineral usually deriving from the reaction of carbonaceous minerals with the metabolic products secreted by microbiological organisms, especially fungi [82,83], confirming the attribution of the infrared band at 1610 cm^{-1} to an increse in oxalic acid.

On the other hand, bacteria, detected on sample #1 by FISH analyses, may have contributed to the wood carbohydrate depletion and caused a loss of its strength properties associated with an increase in wood porosity and fragility [8]. Clear irregular shapes and small cavities were observed by SEM analyses in the wood structure. These cavities could be attributed to cavitation bacteria, although other, deeper analyses are needed; these cavities started near a pit chamber in the cell wall or directly in other areas within the secondary cell wall [1,25].

Another deterioration factor was the prolonged interaction of archaeological wood with the burial soil and the fluctuation of the humidity rate of the burial environment. During the rainy seasons, the increase in the water amount soaking the soil can cause the dissolution of its mineral components. XRD measurements demonstrated that the analysed soil was composed by a very high amount of soluble salts (especially halite, NaCl) and several minerals, such as carbonates, gypsum, and silicates. A water solution saturated with dissolved mineral components deeply penetrated the statue body causing wood swelling.

During the dry seasons, as a consequence of a decrease in humidity rate inside the burial pit, a recrystallisation of the mineral components may have taken place, leading to an increase in the wood volume. This hypothesis was confirmed by XRD measurements, revealing that the mineral composition of soil collected from the core of the statue (sample #6) was comparable to that of soil collected from the thick petrified outer soil layer enveloping the statue at the time of its discovery (sample #5). Following cycles of wood swelling and shrinkage could have caused the severe cracking and collapsing of the wood structures both at microscopic (as shown by SEM images) and macroscopic levels [84].

The composition (mainly calcite) of the soil sample #5 enveloping the statue is attributed to the limestone environment of the archaeological site. Limestone, as in our case, has a high pH value that can inhibit the growth of fungi. High pH may cause bacterial growth, thanks to the high pH tolerance, especially for some species already found in waterlogged archaeological wood [85–87]. The alkaline environment is also responsible for initiating the physical and chemical deterioration that may change the properties of the wood [2,24,65,80].

The element analysis by XRD measurements showed the presence of Ca, Si, Cl, and Na in the ancient wood. This could be ascribed to the penetrated soil components into the wood, while the presence of S might have been due to the biotic deterioration effects [88]. These assumptions for the wood deterioration and the role of soil in this process have already been found by other authors for ancient wood saturated with water and buried objects in soil [89–95].

5. Conclusions

The complex scenario of the deterioration processes taking place on the ancient and valuable wooden statue of King Djedefre coming from the archaeological contexts of Abu-Rawash is here described. The burial of the statue for thousands of years in a moist environment led to relatively enormous changes in physico-chemical properties of wood due to biotic and abiotic factors, as revealed by different advanced analyses applied to both soil and wooden samples. An increase in porosity, fragility, and inhomogeneity of the wooden structure was found by SEM analyses, and a reduction in carbon percentage of the ancient wood samples compared to the standard ones was revealed by EDX. This was probably due to chemoorganotrophic bacteria and fungi that use the organic substrates as hydrogen, carbon, and energy, a source for microorganisms that release complexing biocorrosive organic acids. The chemical analysis of wood, soil, and limestone samples by XRD confirmed the presence of weddellite, halite, quartz, and kaolinite in wood and soil samples, while calcite, gypsum, halite, and quartz appeared in the limestone sample. Extreme cellulose dissociation in the ancient wooden samples was also observed. Microbiological analyses of wood (by FISH and PCR) identified bacteria as one of the biotic factors that accelerate the wood deterioration.

An accurate study of these concomitant variables, as well as the effects they can produce on ancient objects, are the first key step for increasing the knowledge for planning the appropriate conservation procedures for this wood statue and to allow for planning the best strategies to preserve the integrity of the archaeological artefacts. The archaeological significance of the statue goes beyond being a royal statue. A careful reading of the hidden signs tells us a lot about ancient life in Egypt, whether it was religious or commercial. The statue emphasises the role of women in this period. It is clear that the statue depicted a woman of religious standing, probably writing religious texts, although deeper investigations are needed.

Finally, the development of new cleaning techniques and the formulation of innovative chemical products for disinfestation, consolidation, and restoration will allow this artefact to be available for future generations. It will be placed within an amazing museum context such as the soon-opening Grand Egyptian Museum of Giza where the sitting scribe statue will find its forever place and where it will answer some questions that have been tackled by Egyptologists.

Supplementary Materials: The following supporting information can be downloaded at https://www.mdpi.com/article/10.3390/app12147020/s1, Figure S1. Infrared spectra of the soil samples #4 (Inner the statue, red), #5 (Petrified outer layer, white) and #6 (Inner the statue, dark grey). The coloured selections highlight the characteristic infrared features of carbonates, sulphates and silicate. Among silicates, the presence of kaolinite can be distinguished by the sharp absorptions in the 3750–3500 cm^{-1} range. Figure S2: XRD patterns of the soil samples #4 (a), #5 (b) and #6 (c). Table S1: Estimated chemical composition of the soil and wooden samples by X-ray diffraction technique.

Author Contributions: Writing—original draft preparation, D.M.A., S.I. and P.G.; writing—review and editing, C.S., G.B., N.A., E.A., L.V., A.V., Y.B. and W.S.; data curation, D.M.A., S.I., C.S., G.B., L.V. and P.G.; funding acquisition, Y.B.; supervision, Y.B. and W.S. All authors have read and agreed to the published version of the manuscript.

Funding: We acknowledge the International Center for Theoretical Physics (ICTP) for financial support under the ICTP-Elettra Users Programme for access to Elettra Sincrotrone Trieste (SISSI-Chem-Life Sci) beam line (proposal No. 20195552).

Institutional Review Board Statement: Not applicable.

Informed Consent Statement: The approval of this work was granted by the Permanent Committee of the Egyptian Ministry of Tourism and Antiquities to the authors from Egypt. All necessary permits were obtained for the described study, which complied with all relevant regulations.

Data Availability Statement: Not applicable.

Acknowledgments: The Egyptian authors would like to acknowledge the Yehia Badr, supervisor of D.M.A., recently passed away. May God have mercy on him and forgive him and dwell in his vast paradise.

Conflicts of Interest: The authors declare no conflict of interest.

References

1. Blanchette, A.R. A review of microbial deterioration found in archaeological wood from different environments. *Int. Biodeterior. Biodegrad.* **2000**, *46*, 189–204. [CrossRef]
2. Blanchette, R.A.; Nilsson, T.; Daniel, G.; Abad, A. Biological Degradation of Wood. In *Archaeological Wood Properties, Chemistry, and Preservation, Advances in Chemistry Series*; Rowell, R.M., Barbour, J., Eds.; American Chemical Society: Washington, DC, USA, 1990; Volume 225, pp. 141–174.
3. Abdel-Azeem, A.; Held, B.W.; Richards, J.E.; Davis, S.; Blanchette, R.A. Assessment of biodegradation in ancient archaeological wood from the Middle Cemetery at Abydos, Egypt. *PLoS ONE* **2019**, *14*, e0213753. [CrossRef] [PubMed]
4. Pournou, A. *Biodeterioration of Wooden Cultural Heritage*; Springer International Publishing: Cham, Switzerland, 2020; ISBN 978-3-030-46503-2.
5. Branysova, T.; Demnerova, K.; Durovic, M.; Stiborova, H. Microbial biodeterioration of cultural heritage and identification of the active agents over the last two decades. *J. Cult. Herit.* **2022**, *55*, 245–260. [CrossRef]
6. Zisi, A. Forest Wood through the Eyes of a Cultural Conservator. *Forests* **2021**, *12*, 1001. [CrossRef]
7. Pinna, D. Microbial Growth and its Effects on Inorganic Heritage Materials. In *Microorganisms in the Deterioration and Preservation of Cultural Heritage*; Joseph, E., Ed.; Springer International Publishing: Cham, Switzerland, 2021; pp. 3–35. ISBN 978-3-030-69410-4.
8. Broda, M.; Hill, C.A.S. Conservation of Waterlogged Wood—Past, Present and Future Perspectives. *Forests* **2021**, *12*, 1193. [CrossRef]
9. Moosavinejad, S.M.; Madhoushi, M.; Vakili, M.; Rasouli, D. Evaluation of degradation in chemical compounds of wood in historical buildings using FT-IR and FT-Raman vibrational spectroscopy. *Maderas-Cienc. Tecnol.* **2019**, *21*, 381–392. [CrossRef]
10. Ghavidel, A.; Scheglov, A.; Karius, V.; Mai, C.; Tarmian, A.; Vioel, W.; Vasilache, V.; Sandu, I. In-depth studies on the modifying effects of natural ageing on the chemical structure of European spruce (*Picea abies*) and silver fir (*Abies alba*) woods. *J. Wood Sci.* **2020**, *66*, 77. [CrossRef]
11. Antonelli, F.; Esposito, A.; Galotta, G.; Petriaggi, B.D.; Piazza, S.; Romagnoli, M.; Guerrieri, F. Microbiota in Waterlogged Archaeological Wood: Use of Next-Generation Sequencing to Evaluate the Risk of Biodegradation. *Appl. Sci.* **2020**, *10*, 4636. [CrossRef]
12. Goodell, B.; Qian, Y.; Jellison, J. Fungal Decay of Wood: Soft Rot—Brown Rot—White Rot. In *Development of Commercial Wood Preservatives: Efficacy, Environmental, and Health Issues*; Schultz, T.P., Militz, H., Freeman, M.H., Goodell, B., Nicholas, D.D., Eds.; American Chemical Society: Washington, DC, USA, 2008; pp. 9–31.
13. Singh, A.P.; Kim, Y.S.; Chavan, R.R. Advances in Understanding Microbial Deterioration of Buried and Waterlogged Archaeological Woods: A Review. *Forests* **2022**, *13*, 394. [CrossRef]

14. Pedersen, N.B.; Matthiesen, H.; Blanchette, R.A.; Alfredsen, G.; Held, B.W.; Westergaard-Nielsen, A.; Hollesen, J. Fungal attack on archaeological wooden artefacts in the Arctic—Implications in a changing climate. *Sci. Rep.* **2020**, *10*, 14577. [CrossRef]
15. Bari, E.; Daryaei, M.G.; Karim, M.; Bahmani, M.; Schmidt, O.; Woodward, S.; Ghanbary, M.A.T.; Sistani, A. Decay of *Carpinus betulus* wood by *Trametes versicolor*—An anatomical and chemical study. *Int. Biodeterior. Biodegrad.* **2018**, *137*, 68–77. [CrossRef]
16. Schmidt, O.; Bahmani, M.; Koch, G.; Potsch, T.; Brandt, K. Study of the fungal decay of oil palm wood using TEM and UV techniques. *Int. Biodeterior. Biodegrad.* **2016**, *111*, 37–44. [CrossRef]
17. Bari, E.; Daniel, G.; Yilgor, N.; Kim, J.S.; Tajick-Ghanbary, M.A.; Singh, A.P.; Ribera, J. Comparison of the Decay Behavior of Two White-Rot Fungi in Relation to Wood Type and Exposure Conditions. *Microorganisms* **2020**, *8*, 1931. [CrossRef] [PubMed]
18. Brischke, C.; Alfredsen, G. Wood-water relationships and their role for wood susceptibility to fungal decay. *Appl. Microbiol. Biotechnol.* **2020**, *104*, 3781–3795. [CrossRef] [PubMed]
19. Huisman, D.; Manders, M.; Kretschmar, E.; Klaassen, R.; Lamersdorf, N. Burial conditions and wood degradation at archaeological sites in the Netherlands. *Int. Biodeterior. Biodegrad.* **2008**, *61*, 33–44. [CrossRef]
20. Kim, Y.S.; Singh, A.P. Micromorphological characteristics of wood biodegradation in wet environments: A review. *IAWA J.* **2000**, *21*, 135–155. [CrossRef]
21. Johnston, S.R.; Boddy, L.; Weightman, A. Bacteria in decomposing wood and their interactions with wood-decay fungi. *FEMS Microbiol. Ecol.* **2016**, *92*, fiw179. [CrossRef]
22. Daniel, G. Microview of Wood under Degradation by Bacteria and Fungi. In *Wood Deterioration and Preservation: Advances in Our Changing World*; Goodell, B., Nicholas, D.D., Schultz, T.P., Eds.; ACS Symposium Series 845; Oxford University Press: Oxford, UK, 2003; pp. 34–72.
23. Daniel, G.F.; Nilsson, T.; Singh, A.P. Degradation of lignocellulosics by unique tunnel-forming bacteria. *Can. J. Microbiol.* **1987**, *33*, 943–948. [CrossRef]
24. Singh, A.P.; Butcher, J. Bacterial degradation of wood cells: A review of degradation patterns. *J. Inst. Wood Sci.* **1991**, *12*, 143–157.
25. Björdal, C.; Nilsson, T.; Daniel, G. Microbial decay of waterlogged archaeological wood found in Sweden Applicable to archaeology and conservation. *Int. Biodeterior. Biodegrad.* **1999**, *43*, 63–73. [CrossRef]
26. Kibblewhite, M.; Tóth, G.; Hermann, T. Predicting the preservation of cultural artefacts and buried materials in soil. *Sci. Total Environ.* **2015**, *529*, 249–263. [CrossRef] [PubMed]
27. De Jong, J. Conservation Techniques for Old Waterlogged Wood from Shipwrecks Found in the Netherlands. *Biodeterior. Invest. Tech.* **1977**, 295–338.
28. McConnachie, G.; Eaton, R.; Jones, M. A re-evaluation of the use of maximum moisture content data for assessing the condition of waterlogged archaeological wood. *e-Preserv. Sci.* **2008**, *5*, 29–35.
29. Gelbrich, J.; Mai, C.; Militz, H. Chemical changes in wood degraded by bacteria. *Int. Biodeterior. Biodegrad.* **2008**, *61*, 24–32. [CrossRef]
30. Kim, Y.S.; Singh, A.P. Wood as cultural heritage material and its deterioration by biotic and abiotic agents. In *Secondary Xylem Biology Origins, Functions, and Applications*; Kim, I.S., Funada, R., Singh, A.P., Eds.; Academic Press: New York, NY, USA, 2016; pp. 233–257.
31. Ghavidel, A.; Hosseinpourpia, R.; Militz, H.; Vasilache, V.; Sandu, I. Characterization of Archaeological European White Elm (*Ulmus laevis* P.) and Black Poplar (*Populus nigra* L.). *Forests* **2020**, *11*, 1329. [CrossRef]
32. Ghavidel, A.; Hofmann, T.; Bak, M.; Sandu, I.; Vasilache, V. Comparative archaeometric characterization of recent and historical oak (*Quercus* spp.) wood. *Wood Sci. Technol.* **2020**, *54*, 1121–1137. [CrossRef]
33. Popescu, C.-M.; Tibirna, C.-M.; Vasile, C. XPS characterization of naturally aged wood. *Appl. Surf. Sci.* **2009**, *256*, 1355–1360. [CrossRef]
34. Pyzik, A.; Ciuchcinski, K.; Dziurzynski, M.; Dziewit, L. The Bad and the Good—Microorganisms in Cultural Heritage Environments—An Update on Biodeterioration and Biotreatment Approaches. *Materials* **2021**, *14*, 177. [CrossRef]
35. Liu, X.; Qian, Y.; Wang, Y.; Wu, F.; Wang, W.; Gu, J.-D. Innovative approaches for the processes involved in microbial biodeterioration of cultural heritage materials. *Curr. Opin. Biotechnol.* **2022**, *75*, 102716. [CrossRef]
36. Raynaud, S.; De La Boisse, H.; Makroum, F.M.; Bertho, J. Geological and topographical study of the original hills at the base of Fourth Dynasty Egyptian monuments of the Memphite plateau. *Bull. Soc. Geol. Fr.* **2010**, *181*, 279–290. [CrossRef]
37. Moneim, A.A.A. Overview of the geomorphological and hydrogeological characteristics of the Eastern Desert of Egypt. *Appl. Hydrogeol.* **2004**, *13*, 416–425. [CrossRef]
38. Redford, D.B. *The Oxford Encyclopedia of Ancient Egypt*; Oxford University Press: Oxford, UK, 2001; ISBN 9780195102345.
39. Shaw, I.; Nicholson, P. *British Museum Dictionary of Ancient Egypt*; The American University in Cairo Press: Cairo, Egypt, 1995; ISBN 2560007480451.
40. Shaw, I. *The Oxford History of Ancient Egypt*; Oxford University Press: Oxford, UK, 2000; ISBN 9780192802934.
41. Helck, W. *Untersuchungen zur Thinitenzeit*; Otto Harrassowitz: Wiesbaden, Germany, 1987; ISBN 9783447026772.
42. Hawass, Z.A. Archaic Graves Recently Found at North Abu Roash. Mitteilungen des Dtsch. *Archäologischen Instituts Abteilung Kairo* **1980**, *36*, 229–244.
43. Bagnall, R.S.; Brodersen, K.; Champion, C.B.; Erskine, A.; Huebner, R.S. *The Encyclopedia of Ancient History*; Wiley-Blackwell: Malden, MA, USA, 2012; ISBN 9781405179355.

44. Xiong, J.; Li, A.; Liu, C.; Dong, J.; Yang, B.; Cao, J.; Ren, T. Probing the historic thermal and humid environment in a 2000-year-old ancient underground tomb and enlightenment for cultural heritage protection and preventive conservation. *Energy Build.* **2021**, *251*, 111388. [CrossRef]
45. Galotta, G.; Nugari, M.P.; Flamini, M.G. Il degrado biologico di alcuni prodotti derivati del legno da utilizzare in aree archeologiche. *Boll. ICR Nuova Ser.* **2002**, *5*, 139–150.
46. Galotta, G. *Studi di Caratterizzazione per la Conservazione dei Manufatti Lignei Provenienti dalle Aree di Scavo Vesuviane*; Università degli Studi di Firenze: Florence, Italy, 1999.
47. Wheeler, E.A. Inside Wood—A Web resource for hardwood anatomy. *IAWA J.* **2011**, *32*, 199–211. [CrossRef]
48. Rambo, M.K.D.; Ferreira, M.M.C. Determination of Cellulose Crystallinity of Banana Residues Using Near Infrared Spectroscopy and Multivariate Analysis. *J. Braz. Chem. Soc.* **2015**, *26*, 1491–1499. [CrossRef]
49. Andersson, S.; Serimaa, R.; Paakkari, T.; Saranpää, P.; Pesonen, E. Crystallinity of wood and the size of cellulose crystallites in Norway spruce (*Picea abies*). *J. Wood Sci.* **2003**, *49*, 531–537. [CrossRef]
50. Franceschi, E. X-ray Diffraction in Cultural Heritage and Archaeology Studies. *Open Access Libr. J.* **2014**, *1*, 1–10. [CrossRef]
51. Segal, L.; Creely, J.J.; Martin, A.E., Jr.; Conrad, C.M. An Empirical Method for Estimating the Degree of Crystallinity of Native Cellulose Using the X-ray Diffractometer. *Text. Res. J.* **1959**, *29*, 786–794. [CrossRef]
52. Birarda, G.; Bedolla, D.; Piccirilli, F.; Stani, C.; Vondracek, H.; Vaccari, L. Chemical analyses at micro and nano scale at SISSI-Bio beamline at Elettra-Sincrotrone Trieste. *Proc. SPIE* **2022**, *2022*, 1195707.
53. Cardoni, M.; Barra Caracciolo, A.; Grenni, P. Fluorescence In Situ Hybridization Technique: A Tool Useful for Detecting Cultural Heritage Biodeteriogens. In *Sciences and Technologies applied to Cultural Heritage I (STACH 1)*; Baldi, M., Capriotti Vittozzi, G., Eds.; Consiglio Nazionale delle Ricerche, Centro Archeologico Italiano—Istituto Italiano di Cultura: Rome, Italy, 2019; pp. 37–46. ISBN 978 88 8080 347 8.
54. Amann, R.; Fuchs, B.M. Single-cell identification in microbial communities by improved fluorescence in situ hybridization techniques. *Nat. Rev. Microbiol.* **2008**, *6*, 339–348. [CrossRef] [PubMed]
55. Caracciolo, A.B.; Grenni, P.; Cupo, C.; Rossetti, S. In situ analysis of native microbial communities in complex samples with high particulate loads. *FEMS Microbiol. Lett.* **2005**, *253*, 55–58. [CrossRef] [PubMed]
56. Greuter, D.; Loy, A.; Horn, M.; Rattei, T. probeBase—An online resource for rRNA-targeted oligonucleotide probes and primers: New features 2016. *Nucleic Acids Res.* **2015**, *44*, D586–D589. [CrossRef] [PubMed]
57. McKinney, C.W.; Dungan, R.S.; Moore, A.; Leytem, A.B. Occurrence and abundance of antibiotic resistance genes in agricultural soil receiving dairy manure. *FEMS Microbiol. Ecol.* **2018**, *94*, fiy010. [CrossRef]
58. Ludwig, W. Nucleic acid techniques in bacterial systematics and identification. *Int. J. Food Microbiol.* **2007**, *120*, 225–236. [CrossRef]
59. Harvey, J. Wooden Statuary. In *UCLA Encyclopedia of Egyptology*; Wendrich, W., Ed.; John Wiley and Sons Ltd.: Los Angeles, CA, USA, 2009.
60. Lucas, A. *Ancient Egyptian Materials and Industries*; Edward Arnold: London, UK, 1948.
61. Bard, K.A. *An Introduction to the Archaeology of Ancient Egypt*; Wiley-Blackwell: New York, NY, USA, 2015; ISBN 978-1-405-11148-5.
62. Volkov, D.S.; Rogova, O.B.; Proskurnin, M.A. Organic Matter and Mineral Composition of Silicate Soils: FTIR Comparison Study by Photoacoustic, Diffuse Reflectance, and Attenuated Total Reflection Modalities. *Agronomy* **2021**, *11*, 1879. [CrossRef]
63. Yassin, Z.; El Hadidi, N.N.; Mohamed, M.F. Examination and analyses of a wooden face at the museum storage at the faculty of archaeology, Cairo University. *Mediterr. Archaeol. Archaeom.* **2016**, *16*, 1–11. [CrossRef]
64. Kumar, R.; Sivaganesan, S.; Senthamaraikannan, P.; Saravanakumar, S.S.; Khan, A.; Daniel, S.A.A.; Loganathan, L. Characterization of New Cellulosic Fiber from the Bark of *Acacia nilotica* L. Plant. *J. Nat. Fibers* **2020**, *19*, 199–208. [CrossRef]
65. Lionetto, F.; Del Sole, R.; Cannoletta, D.; Vasapollo, G.; Maffezzoli, A. Monitoring Wood Degradation during Weathering by Cellulose Crystallinity. *Materials* **2012**, *5*, 1910–1922. [CrossRef]
66. Burattini, S.; Falcieri, E. Scanning and transmission electron microscopy in cultural heritage: State of the art. *Microscopie* **2020**, *31*, 9183. [CrossRef]
67. Elgat, W.A.A.A.; Taha, A.S.; Salem, M.Z.M.; Fares, Y.G.D.; Böhm, M.; Mohamed, M.F.; Nasser, R.A.; Pommer, V. The Effects of Iron Rust on the Ageing of Woods and Their Derived Pulp Paper. *Polymers* **2021**, *13*, 3483. [CrossRef] [PubMed]
68. Gelbrich, J.; Mai, C.; Militz, H. Evaluation of bacterial wood degradation by Fourier Transform Infrared (FTIR) measurements. *J. Cult. Herit.* **2012**, *13*, S135–S138. [CrossRef]
69. Dixon, D.M. Timber in ancient Egypt. *Commonw. For. Rev.* **1974**, *53*, 205–209.
70. Moreno García, J.C. War in Old Kingdom Egypt (2686-2125 BCE). In *Studies on War in the Ancient Near East. Collected Essays on Military History (AOAT, 372)*; Vidal, J., Ed.; Ugarit Verlag: Münster, Germany, 2010; pp. 5–41.
71. Allen, J.P. *Egyptian Art in the Age of the Pyramids*; Metropolitan Museum of Art: New York, NY, USA, 1999; ISBN 978-0300199727.
72. Russmann, E.R. *Egyptian Sculpture: Cairo and Luxor*; University of Texas Press: Austin, TX, USA, 1989; ISBN 9780714109534.
73. Robins, G. Hair and the Construction of Identity in Ancient Egypt, c. 1480–1350 B.C. *J. Am. Res. Cent. Egypt* **1999**, *36*, 55. [CrossRef]
74. David, R. *Religion and Magic in Ancient Egypt*; Penguin Publishing Group: New York, NY, USA, 2002; ISBN 978-0140262520.
75. Van der Horst, P.W. The way of Life of the Egyptian Priests According to Chaeremon. In *Studies in Egyptian Religion Dedicated to Professor Jan Zandee*; Brill Academic Publishers: Leiden, The Netherlands, 1982; pp. 61–71.
76. Gosline, S.L. Female Priests: A Sacerdotal Precedent from Ancient Egypt. *J. Fem. Stud. Relig.* **1996**, *12*, 25–39.

77. Budin, S.L.; Turfa, J.M. (Eds.) *Women in Antiquity*; Routledge: London, UK, 2016; ISBN 9781315621425.
78. Mahmoud, H.M. A Female Scribe in the Twenty Sixth Dynasty (Iretrau). *J. Gen. Union Arab Archaeol.* **2018**, *1*, 54–74. [CrossRef]
79. Harvey, J.C. Typological Study of Egyptian Wooden Statues of Old Kingdom. Ph.D. Dissertation, University College London, London, UK, 1994.
80. Tamburini, D.; Cartwright, C.R.; Cofta, G.; Zborowska, M.; Mamoňová, M. Distinguishing the Signs of Fungal and Burial-Induced Degradation in Waterlogged Wood from Biskupin (Poland) by Scanning Electron Microscopy. *Microsc. Microanal.* **2018**, *24*, 163–182. [CrossRef]
81. Liu, G.-L.; Kazarian, S.G. Recent advances and applications to cultural heritage using ATR-FTIR spectroscopy and ATR-FTIR spectroscopic imaging. *Analyst* **2022**, *147*, 1777–1797. [CrossRef]
82. Burford, E.P.; Kierans, M.; Gadd, G.M. Geomycology: Fungi in mineral substrata. *Mycologist* **1999**, *17*, 98–107. [CrossRef]
83. Warscheid, T.; Braams, J. Biodeterioration of stone: A review. *Int. Biodeterior. Biodegrad.* **2000**, *46*, 343–368. [CrossRef]
84. Walsh-Korb, Z.; Avérous, L. Recent developments in the conservation of materials properties of historical wood. *Prog. Mater. Sci.* **2018**, *102*, 167–221. [CrossRef]
85. Blanchette, R.A.; Simpson, E. Soft Rot and Wood Pseudomorphs in an Ancient Coffin (700 Bc) From Tumulus Mm at Gordion, Turkey. *IAWA J.* **1992**, *13*, 201–213. [CrossRef]
86. Blanchette, R.A.; Obst, J.R.; Timell, T.E. Biodegradation of Compression Wood and Tension Wood by White and Brown Rot Fungi. *Holzforschung* **1994**, *48*, 34–42. [CrossRef]
87. Liu, Z.; Fu, T.; Hu, C.; Shen, D.; Macchioni, N.; Sozzi, L.; Chen, Y.; Liu, J.; Tian, X.; Ge, Q.; et al. Microbial community analysis and biodeterioration of waterlogged archaeological wood from the Nanhai No. 1 shipwreck during storage. *Sci. Rep.* **2018**, *8*, 7170. [CrossRef]
88. Mansour, M.; Hassan, R.; Salem, M. Characterization of historical bookbinding leather by FTIR, SEM-EDX and investigation of fungal species isolated from the leather. *Egypt. J. Archaeol. Restor. Stud.* **2017**, *7*, 1–10. [CrossRef]
89. Donaldson, L.A.; Singh, A.P. Ultrastructure of Terminalia Wood from an Ancient Polynesian Canoe. *IAWA J.* **1990**, *11*, 195–202. [CrossRef]
90. Blanchette, R.A.; Held, B.W.; Jurgens, J.A.; Haight, J.E. Wood deterioration in Chacoan great houses of the southwestern United States. *Conserv. Manag. Archaeol. Sites* **2004**, *6*, 203–212. [CrossRef]
91. Blanchette, R.A.; Held, B.W.; Jurgens, J.A.; McNew, D.L.; Harrington, T.C.; Duncan, S.M.; Farrell, R.L. Wood-Destroying Soft Rot Fungi in the Historic Expedition Huts of Antarctica. *Appl. Environ. Microbiol.* **2004**, *70*, 1328–1335. [CrossRef]
92. Blanchette, R.A.; Held, B.W.; Arenz, B.E.; Jurgens, J.A.; Baltes, N.J.; Duncan, S.M.; Farrell, R.L. An Antarctic Hot Spot for Fungi at Shackleton's Historic Hut on Cape Royds. *Microb. Ecol.* **2010**, *60*, 29–38. [CrossRef]
93. Filley, T.R.; Blanchette, R.A.; Simpson, E.; Fogel, M.L. Nitrogen cycling by wood decomposing soft-rot fungi in the "King Midas tomb," Gordion, Turkey. *Proc. Natl. Acad. Sci. USA* **2001**, *98*, 13346–13350. [CrossRef]
94. Ortiz, R.; Párraga, M.; Navarrete, J.; Carrasco-Wong, I.; De la Vega, E.; Ortiz, M.; Herrera, P.; Jurgens, J.A.; Held, B.W.; Blanchette, R.A. Investigations of Biodeterioration by Fungi in Historic Wooden Churches of Chiloé, Chile. *Microb. Ecol.* **2014**, *67*, 568–575. [CrossRef] [PubMed]
95. Alba, Z.; Sabrina, P.; Massimo, M.; Louis, G.; Gaetan, L.F. Molecular diagnosis by PCR-DHPLC technique of wood-decay fungi in historical buildings in Italy. *Pro Ligno* **2011**, *7*, 92–97.